An experimental study of a parallel-plate radio-frequency discharge: Measurements of the radiation temperature and electron density

G. A. Hebner,[a] J. T. Verdeyen, and M. J. Kushner
Gaseous Electronics Laboratory, University of Illinois at Urbana-Champaign, 607 East Healey, Champaign, Illinois 61820

(Received 22 July 1987; accepted for publication 24 November 1987)

Microwave diagnostic techniques have been used to measure the radiation temperature and electron density in parallel-plate capacitively coupled radio-frequency (2.5 MHz) discharges. Evidence is presented for the existence and importance of an energetic electron beam, produced by the large cathode sheath voltage, which sustains and excites the plasma. The measured radiation temperature of the bulk electrons is 500 K for helium and 800 K for argon. An upper limit on the radiation temperature is obtained for N_2 (1200 K) and CF_4 (3000 K) discharges. Measurements of the electron density in helium as a function of electrode spacing show a peak in the electron density that is consistent with the theory of ionization by beam electrons. The electric fields required to carry the rf current by drift in the bulk of the glow are low and consistent with the measured radiation temperature. The implications of these measurements on the nature of the rf plasma-sustaining mechanism. The voltage distribution, and the electron energy distribution are discussed.

I. INTRODUCTION

The use of radio-frequency (rf) plasmas in the processing of semiconductor materials and devices has increased greatly in the last decade since plasma processing has several advantages, such as anisotropic etch profiles and cleanliness, over conventional liquid processing techniques.[1–4] However, the physics of the rf plasma and the chemical mechanisms of etching or deposition are not well understood. The time-dependent nature of the rf plasma and sheaths, the large number of species present in the plasma, and the hostile experimental environment make nonpertubative experiments and analysis difficult. Despite the difficulty, an experimental and theoretical understanding of the plasma processing discharge is emerging.

Recently, models for the rf plasma have taken several distinct forms. For example, Monte Carlo techniques have been used to model the electron and ion distributions and chemical species production.[5–7] One generally assumes a functional form for the sheath potentials and calculates the electron and ion energy distributions at various positions between the electrodes. These models have the advantage of easily observing the change in the distribution function or chemical species production as a result of the addition or subtraction of a particular process. Several other authors have employed a different approach to modeling rf systems.[8–10] They assume that the electrodes and the rf sheaths can be modeled as two planar probes connecting the plasma. Starting with the fundamental probe theory[11,12] and a consideration of the rf circuit, one can compute plasma properties such as plasma potential, dc bias, and current. The quantitative agreement between theory and experiment is good for low pressures (<100 mT) and low frequencies (<100 kHz). However, one author[10] has noted that the model behaves as if there is an external ionization source. One possible external ionization source will be discussed in Sec. III.

One item that these and other models[13,14] have in common is the use of an average electron energy or electron temperature and a Maxwellian electron energy distribution. In some cases, an electron temperature is assumed to do the calculation, or at best an average electron energy is computed from the calculated electron energy distribution. In either case, the typical value of the average electron energy or temperature is a few electron volts. By virtue of the computational methods used, this temperature is analogous to what one would compute for a positive column plasma.

Since the electron energy is a critical theoretical parameter, it is important to have good experimental justification for its use. Although probes can be inserted into the plasma,[12,15] their interpretation is clouded by the same issue that limits our present models, namely, a good theory of the rf sheath. For instance, if the plasma potential (with respect to the probe reference) has a time-dependent component, then the probe circuit will rectify the voltage, making interpretation of the static *V-I* characteristics difficult. The only other alternative, at present, is to use indirect evidence of the average electron energy and energy distribution. For example, optical emission studies in a helium rf discharge have indicated that the glow is the result of excitation by a high-energy electron beam produced in the cathode sheath.[16] The net effect of the ballistic electrons will be to provide a nonlocal ionization source to the plasma[15,17] and as a consequence reduce the bulk plasma electric field, the electron temperature, and the importance of volume ionization. Due to the time-varying nature of the rf plasma, the relative importance of ballistic electrons and volume ionization is expected to be a function of the excitation frequency. Under discharge conditions where the ballistic electrons are providing a significant fraction of the ionization, a time-averaged negative glow model of the rf discharge, as opposed to a positive column model, is a better first-order approximation. The diffi-

[a] Current address: Sandia National Laboratories, Albuquerque, NM 87185.

 0021-8979/88/072226-11$02.40

culty is that such a view requires a global, rather than a local analysis of the discharge. In any case, a direct measurement of the average electron energy and an indication of the shape of the energy distribution is lacking to validate the models.

We have used microwave diagnostic techniques to directly measure the electron radiation temperature and the electron density of an rf discharge. The radiation temperature of the helium and argon rf plasma was found to be lower than commonly assumed (< 1000 K) and the electron density in helium peaked when the electrode separation was 10–15 cm. These observations indicate that the discharge behaves as if there is an electron beam, originating in the cathode sheath, which produces significant ionization and excitation. Knowing the electron density, its spatial distribution (obtained from the optical emission), and the circuit current, one can assign an upper limit to the electric field in the bulk of the plasma between the sheaths. This field (5.3 mV/cm) is also lower than commonly assumed, though consistent with the measured radiation temperature. While the properties of argon, nitrogen, and CF_4 rf plasmas were investigated, the majority of this work was performed in helium simply because many of the transport parameters were accurately known to facilitate theoretical models. To check the validity of the microwave temperature measurement, the radiation temperature and electron density of a pulsed dc positive column plasma were measured. The measured values are in very good agreement with the values calculated with a two-step ionization model of the positive column.

The experimental setup and brief theory of the measurement are described in Sec. II. The results of measurements of the rf plasma radiation temperature and electron density in He, Ar, N_2, and CF_4 and the implications of these measurements on the characteristics of the discharge are discussed in Sec. III. Conclusions are given in Sec. IV. Due to the unexpectedly low values of the radiation temperature, the accuracy of the microwave system was cross checked against the relatively well-known dc positive column. The calibration procedure is outlined in the Appendix.

II. EXPERIMENTAL SETUP

The rf matching network, microwave system, and discharge tube are shown in Fig. 1. The rf system consists of a signal generator, rf amplifier (ENI 300A), matching network, and parallel-plate discharge chamber. To be consistent with previous studies,[16] most of the work was performed at an rf frequency of 2.5 MHz. The applied rf voltage and current were measured using a Hewlett Packard capacitance voltage divider (1000:1) and a Pearson current probe, respectively, while the rf power was monitored using a Bird in-line wattmeter. The wattmeter power agrees, to within 20%, with the power obtained by calculating a time average of the product of the time-dependent voltage and current. The dc self-bias was measured through an rf filter. The 9-cm-diameter aluminum rf electrodes were mounted in a Pyrex tube so that the electrode separation could be varied. The gas was slowly flowed through the discharge chamber and the pressure (0.05–6.0 Torr) was monitored with an MKS capacitance manometer.

The microwave system shown in Fig. 1 consists of two

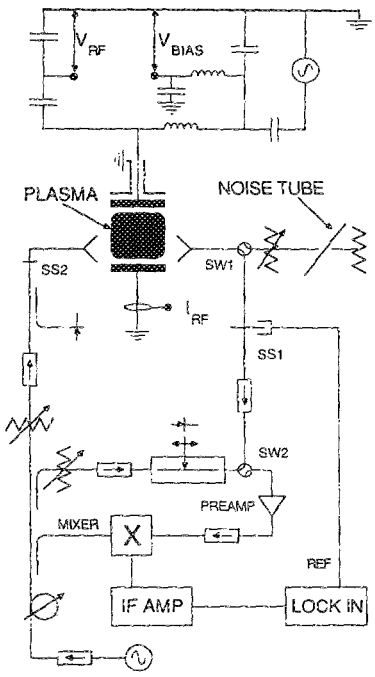

FIG. 1. Schematic of the rf matching network, discharge chamber, and microwave system. The X-band (8.4 GHz) microwave system consists of a microwave interferometer to measure electron density and microwave attenuation and a superheterodyne receiver to measure radiation temperature. SS1 and SS2 are sliding waveguide shorts and SW1 and SW2 are waveguide switches. The rf frequency is 2.5 MHz and the pressure, monitored with a capacitance manometer, is 0.05–6.0 Torr.

subsystems. The first is a microwave interferometer to measure the electron density and microwave attenuation of the plasma. The second is an X band (8.4 GHz) superheterodyne receiver and calibration equipment to measure the microwave noise power emitted by the plasma (referred to as the electron radiation temperature). The position of waveguide switches 1 and 2 (SW1 and SW2) determines which microwave subsystem is in operation. In Fig. 1 the switches are set to measure the electron density and attenuation. The two systems and their theory of operation are described below.

The microwave bridge consists of a reference arm and a plasma arm with the two signals compared in the slotted line. Since the microwaves in the plasma arm traverse the plasma, the position of the standing wave in the slotted line is a function of the phase and insertion loss introduced by the electrons. The phase shift and insertion loss are measured by adjusting the precision attenuator in the reference arm and the slotted line position to produce a null without a plasma. When the plasma is present, the bridge is rebalanced. The difference in the position of the slotted line and the attenuator is related to the phase shift or electron density and the insertion loss of the plasma.

The average electron density, $\bar{N}_e$, is related to the differential phase shift caused by the plasma, $\Delta\phi$, by

$$\bar{N}_e = (2c\omega\epsilon_0/l_p e^2)\,\Delta\phi\,, \tag{1a}$$

where c is the speed of light, ω is the microwave frequency, ϵ_0 is the permittivity of free space, l_p is the plasma length, and e is the electron charge.[18–21] In the expression above, we have assumed that $\nu_m^2 \ll \omega^2 \ll \omega_p^2$, where ω_p is the plasma frequency and ν_m is the collision frequency for momentum transfer. The measured average electron density is related to the average of the electron spatial distribution, $N(r,\theta,z)$,

$$\bar{N}_e = \int N(r,\theta,z)E_0^2\,dV \Big/ \int E_0^2\,dV\,, \tag{1b}$$

where V is the measurement volume and E_0 is the electric field of the microwave probe. In order to relate the peak electron density N_0 to the average electron density, the spatial electron distribution was assumed to be the same as the time-averaged optical emission, measured with a collimated photomultiplier and selected spectral lines, from the plasma. Aside from the sheaths near each electrode, the variation of the emission in the z direction (from electrode to electrode) was minimal; thus, the electron density was assumed to be independent of z. The radial variation was significant (Fig. 2) and by using an Abel transform[22] to compensate for the cylindrical geometry, the optical emission coefficient, and the radial electron distribution were inferred to be a zero-order Bessel function [$N_e(r) = N_0 J_0(r)$].[23] As a result, the peak electron density in the center of the plasma, N_0, is approximately twice the spatially averaged value, $\bar{N}_e$.

In theory, the collision frequency ν_m can be obtained from a measurement of the phase shift and the change in plasma attenuation by

$$\nu_m = \frac{\omega\sqrt{1-(c\Delta\phi/\omega l)}}{8.686}\left|\frac{\Delta(dB)}{\Delta\phi}\right|, \tag{2}$$

where $\Delta(dB)$ is insertion loss of the microwaves traversing the plasma.[19,20] In practice, the measurement of true plasma attenuation is difficult as the microwaves tend to scatter and/or couple to the many plasma modes (coordinated physical motion of the electrons in the plasma). In the case of an open-ended system, such as the type used in this experiment, these effects can be severe. Other investigators have also noted that the attenuation measurement is much more sensitive to plasma geometry effects and prone to error than is the phase measurement.[21] As a result of these difficulties, the uncertainties in the electron temperature derived from the collision frequency tend to be very large. For example, in the course of our experiments, we observed under some conditions changes in transmission and phase shift which would imply anomalously high values of collision frequency ν_m and thus electron temperature, if simple collisional absorption is assumed. It is shown in the Appendix that the phase shift measurement gives electron densities that are consistent with independent measurements of the current, electric field, and implied drift velocity, whereas the insertion loss deviates greatly from the theoretically predicted value even in a positive column. However, the measured radiation temperature agrees with known parameters and theoretical models if the insertion loss is interpreted as the plasma emissivity with suitable corrections for the presence of the glass (see the Appendix). Based upon this success in the dc plasma, a similar interpretation of the plasma insertion loss was used for the rf discharge.

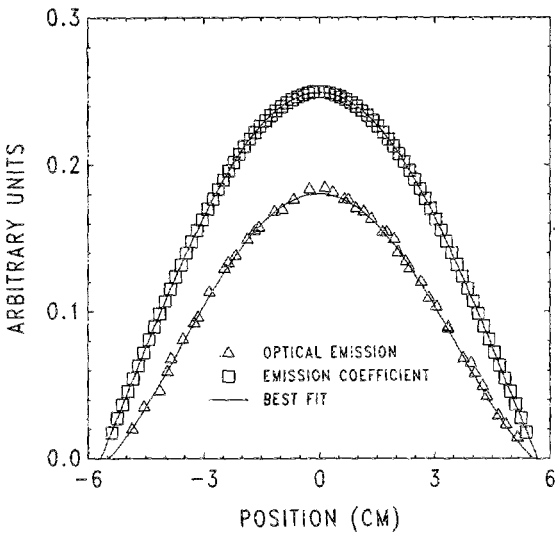

FIG. 2. Time-averaged optical emission for a 0.5-Torr helium rf glow as a function of radial position. The optical emission is measured using an apertured photomultiplier tube. The emission coefficient, which fits a zero-order Bessel function, is computed from the optical emission by using an Abel transform to compensate for the cylindrical geometry.

The microwave noise power is produced by the nearly instantaneous changes in electron velocities due to collisions (Bremsstrahlung) and thus that power reflects the distribution of electron velocities. If that distribution were a Maxwellian, then the amount of power radiated into one electromagnetic mode in a frequency band df (determined by the experimental detection apparatus) is given by

$$P_f = (kT_e\, df)\epsilon(f), \tag{3}$$

where $\epsilon(f)$ is the emissivity of the plasma at the frequency f. Equation (3) is the microwave limit of the Planck's formula for radiation from a "gray" body into one mode. By Kirchoff's law, the emissivity is equal to the absorptivity and thus is a parameter that can be *measured* (as opposed to calculating it—which is also possible).

Unfortunately, the emissivity is also the factor which causes the most difficulty as a few numbers will illustrate. Suppose $kT_e/e = 1$ eV or $T_e = 11\,600$ K and $df = 1$ MHz. If $\epsilon = 1.0$, then a very rudimentary superheterodyne receiver is capable of detecting the power of 1.6×10^{-13} W indicated by the first bracket of Eq. (3). However, if $\epsilon = 0.001$, the noise figure of the receiver must be comparable to 12 K and/or long integration time constants must be employed.

Quite often the format of Eq. (3) is used where T_e is replaced by a radiation temperature T_r for the case of non-Maxwellian plasmas with T_r being given by

$$kT_r = -m\frac{\int R(v)f(v)v^5\,dv}{\int R(v)(\partial f/\partial v)v^4\,dv}, \tag{4a}$$

where m is the electron mass and $f(v)$ is the electron velocity distribution function.[24] The absorption cross section for Bremsstrahlung radiation $R(v)$ is

$$R(v) = [\omega^2 Q_m(v)]/\{\omega^2 + [NvQ_m(v)]^2\}, \tag{4b}$$

where ω is the microwave frequency, N the neutral density, and Q_m the cross section for momentum transfer.[24] In the limit of the microwave frequencies used in these experiments, $R(v) \simeq Q_m(v)$. If, for example, $f(v)$ has a Maxwellian electron energy distribution function, the radiation temperature is equal to the electron temperature ($T_e = T_r$) irrespective of the functional dependence of the cross section on electron energy.[24] For a non-Maxwellian distribution function, the relationship between the radiation temperature and the average electron energy depends on the electron distribution function and the collision cross section.

The emitted noise power was measured using a calibrated superheterodyne receiver which was in operation when the switch SW2 was in the opposite position of that shown in Fig. 1. Microwave noise from either the plasma or the calibrated standard source passed through a motor-driven sliding short (SS1), an isolator, and a low-noise tunnel diode preamplifier ($NF = 4.5$ dB, $G = 16.5$ dB) into a balanced mixer whose output was amplified by the IF strip (General Radio 1216-A) which has a pass band of 0.8 MHz at 30 MHz. The isolators between the balanced mixer, the preamplifier, and the sliding short eliminated any residual local oscillator signal that passed through or reflected from the balanced mixer. Since the receiver was sensitive to powers less than a picowatt, the isolators were used to prevent interference between the reflected signal and local oscillator from changing the operating point of the mixer and overwhelming the detection system. The reference signal (10 Hz) for the lock-in amplifier (PAR 128A) was derived from a chopper wheel attached to the motor driving the sliding short. When the sliding short is across the waveguide, the detected noise power is the characteristic noise of the detection circuit. When the sliding short is open, the IF output is related to the noise power from the plasma. Since the characteristic noise power of the circuit is a constant, the difference between the sliding short being open and closed is proportional to the plasma noise power.

The superheterodyne receiver output was calibrated using a standard microwave noise tube (HP model X347A) and a precision attenuator. The noise tube is an argon plasma with an excess noise figure of 15.4 dB or approximately 10 000 K. The effective source temperature T_s is calculated from

$$T_s = AT_0 + (1 - A)\ 290\ \text{K}, \tag{5}$$

where A is the attenuation of the precision attenuator and T_0 is the temperature of the standard noise tube plasma (10 000 K). The first term represents the power due to the noise tube, while the second is due to the noise emitted by the precision attenuator. In as much as plasma noise is compared to that of a standard with the same receiver, it is not necessary to determine (df) of Eq. (3). A calibration curve for the system is shown in Fig. 3. Due to the low microwave power from the plasma, the effective source temperature is linearly related to the lock-in output voltage. The linear relation between the lock-in signal and temperature is valid for temperatures up to the 10 000-K maximum calibration temperature of the noise tube. In the open-ended system used in these experiments, the minimum detectable excess noise power, due to the laboratory background radiation, was on the order of 300 K. In a closed system, the laboratory background radiation is not measured and the microwave power from a termination at liquid nitrogen (77 K) can easily be detected.

The Pyrex cylinder which contains the plasma also has an effect on the measurement, since the cylinder attenuates the plasma microwave noise and scatters the normal laboratory blackbody background radiation into the receiver horn. To measure the amount of attenuation and scattering, the microwave noise power from several plasma lamps was measured with and without the glass cylinder. Due to the different gas in each lamp, the source temperature of each lamp is different. The source temperature T_s measured without the glass cylinder is assumed to be related to the effective temperature T_e measured with the glass, by

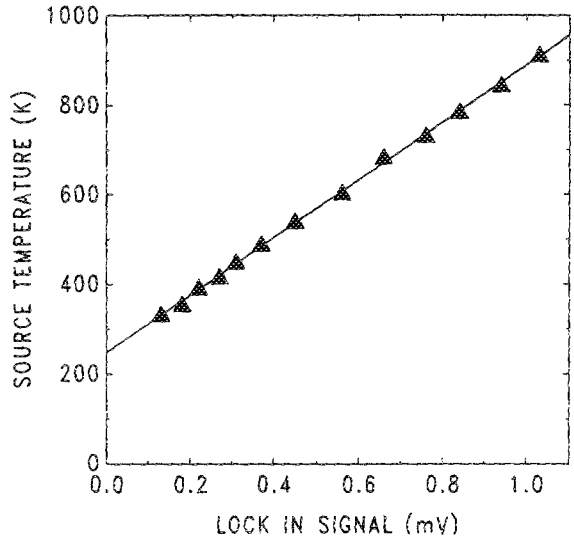

FIG. 3. A calibration curve for the lock-in output voltage showing the effective temperature of the standard noise tube and precision attenuator as a function of lock-in voltage. The linear relation between temperature and voltage continues to at least 10 000 K.

$$T_e = A_g\, T_s + P_s\,, \tag{6}$$

where A_g is the attenuation due to the glass and P_s is the scattered noise from the laboratory background. By using several spectral lamps and measuring the source and effective temperatures, values for A_g (0.41) and P_s (165 K) can be calculated (Fig. 4). The calibrations of A_g and P_s were relatively insensitive to the location of the spectral lamp within the cylinder and the values of A_g and P_s also agree with other indirect measurements. The transmission coefficient of 0.41 corresponds to an attenuation of 3.9 dB which is approximately half the insertion loss measured by propagating a wave across a complete glass cylinder. In addition, the measured scattered noise power (165 K) is approximately equal to the expected noise power from the glass: 290 K$\times$(1–0.41) = 171 K.

The measured noise power from the rf plasma is also a function of the spatial distribution of the electrons and the gain function of the receiving horn.[19–21] The gain function was measured by moving a 0.5-cm-diam Teflon rod across the horn aperture and monitoring the phase shift. The resulting gain function was normalized and agreed with reference data on horn patterns.[21] The spatial distribution of the electrons is assumed to be related to the optical emission coefficient. As previously discussed, the optical emission coefficient, computed from an Abel transform of the optical emission, corresponds to a zero-order Bessel function in the radial direction and is uniform along the axis from electrode to electrode. Assigning an effective temperature to the antenna T_A, the normalization integral is

$$T_A = \frac{1}{4\pi} \int_{4\pi} I(\theta,\varphi) G(\theta,\varphi)\, d\Omega\,, \tag{7}$$

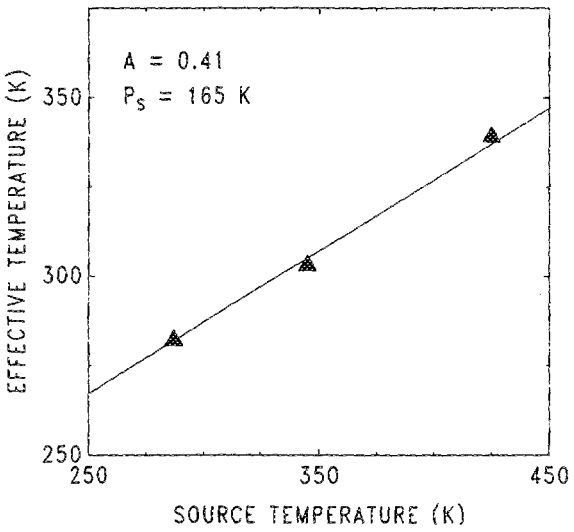

FIG. 4. The effective temperature of the calibration plasma source with the Pyrex cylinder as a function of the source temperature without the cylinder. The straight line is the best linear fit with a slope of 0.41 and an intercept of 165 K.

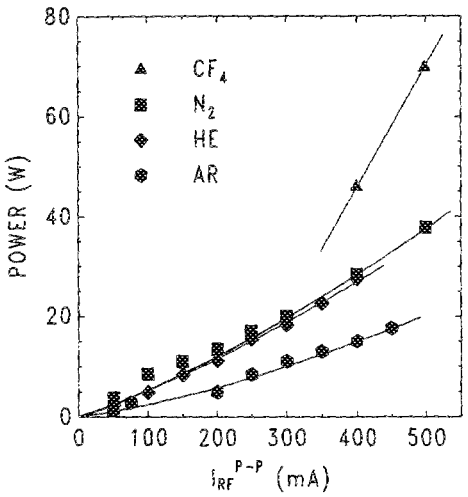

FIG. 6. Power into the plasma as a function of peak-to-peak rf current for helium (0.5 Torr), argon (0.2 Torr), nitrogen (0.09 Torr), and CF_4 (0.045 Torr). Power into the plasma is computed by subtracting the reflected power from the incident power as measured by an in-line wattmeter. The electrode spacing is 9.0 cm.

where $G(\theta,\varphi)$ is the horn gain function and $I(\theta,\varphi)$ is the electron spatial distribution. For the measured $I(\theta,\varphi)$ and $G(\theta,\varphi)$, $T_A = 1.23\ T_0$, where T_0 is the source temperature. Thus, the microwave noise power from the plasma must be multiplied by a factor of 1.23 to compensate for the geometry of the open-ended system.

III. RESULTS AND DISCUSSION

A. Helium

The electron density in a 0.5-Torr helium rf discharge as a function of rf current is shown in Fig. 5 for an electrode spacing of 9.0 cm. With increasing current, the peak-to-peak rf voltage varied between 800 and 1600 V while the dc self-bias was -95 to -240 V. Above approximately 150 mA (2.1 mA/cm^2), the electron density increased linearly with the peak-to-peak current. The power into the discharge, calculated by subtracting the reflected power from the incident power as measured by the in-line wattmeter, is shown in Fig. 6 for several gases and pressures.

As shown in Fig. 7, the radiation temperature of the helium rf discharge was approximately 500 K for currents above 300 mA while the microwave noise power for currents less than 300 mA was below the detection limit of the superheterodyne receiver. The discharge conditions were the same as the previous electron density data (Fig. 5). The temperatures have been compensated for the attenuation and scattering of the Pyrex cylinder and the geometry of the open-ended system. For the conditions shown, the insertion

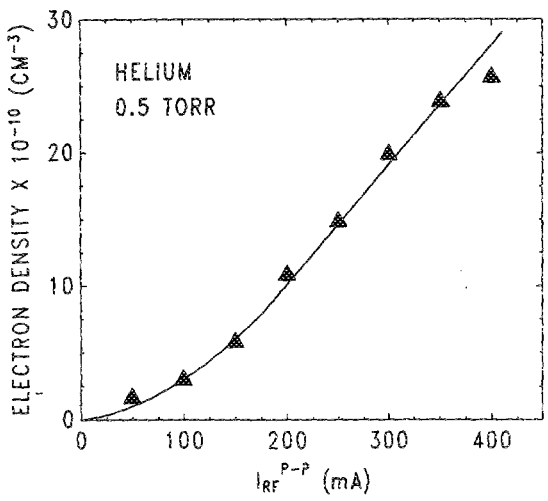

FIG. 5. Electron density as a function of peak-to-peak rf current in a 0.5-Torr helium rf discharge. The peak-to-peak rf voltage is 800–1500 V for an electrode spacing of 9.0 cm.

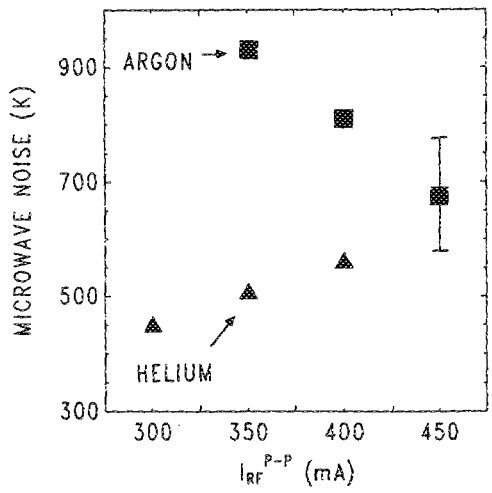

FIG. 7. rf plasma radiation temperature in helium (0.5 Torr) and argon (0.2 Torr) for currents greater than 300 mA. The radiation temperature for currents less than 300 mA is below the detection limit of the superheterodyne receiver. The radiation temperature has been corrected for the attenuation and scattering effects of the Pyrex cylinder enclosing the plasma and the system geometry. The uncertainty in the argon temperature is due to the uncertainty in the insertion loss.

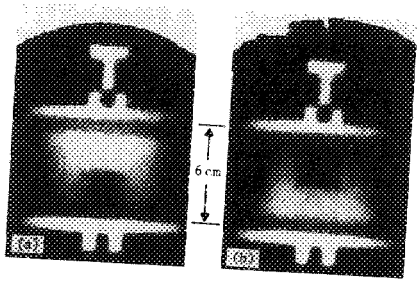

FIG. 8. Framing camera photographs of the 5875-Å helium glow, with a quartz slide in the middle of the discharge, at two phases of the rf period (from Ref. 16). In (a) the driven electrode, marked with a T, is at maximum negative voltage, while (b) is at maximum positive voltage. Discharge conditions are 0.5 Torr, 4.5 W, 350 V_{peak}, 1.0 MHz, and electrode separation of 6.1 cm. The white bands indicate the position of the electrodes.

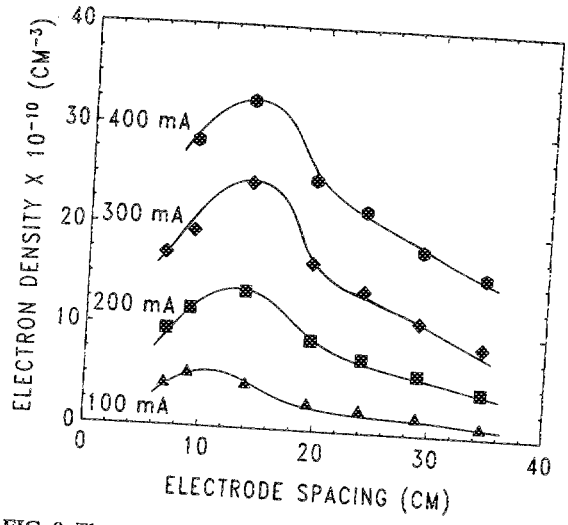

FIG. 9. Electron density of a helium rf plasma (0.5 Torr) as a function of electrode separation for constant peak-to-peak rf current. The peak-to-peak rf voltage is shown in Fig. 10.

loss was greater than 12 dB. As a result, the emissivity factor in Eq. (3) is in the order of 1.

As previously stated, early experimental data in helium have indicated that the glow is produced by a beam of high-energy electrons.[16] In review, when a quartz slide was placed in the middle of an rf discharge, a very distinct dark area was observed on the anode or downstream side of the slide (Fig. 8). The glow region on the cathode or upstream side of the slide was unaffected by the presence of the slide. In addition, the position of the dark area changed as a function of the phase so that the dark space was always on the side of the slide away from the cathode. The conclusion was that the helium rf discharge has some of the characteristics of an electron beam sustained discharge. The electron beam is probably the result of ion bombardment of the cathode and the subsequent acceleration of the secondary electrons across the sheath potential or the acceleration of the bulk electrons by the oscillating sheath boundary.

The data in Fig. 7 support the hypothesis that there is an electron beam component of the electron energy distribution. In an electron beam sustained discharge, a significant fraction of the ionization events are due to collisions of the energetic electron beam with a neutral. Due to the energy of the electron beam (<1 kV), the resulting secondary electron is of relatively low energy (few eV) (Ref. 25) and rapidly relaxes to lower energy due to collisions. For example, the secondary electron has a lifetime, dictated by ambipolar diffusion, of approximately 50 μs.[26] If elastic collisions dominate, the energy relaxation time constant $\tau_e = (G\nu_m)^{-1}$ is approximately equal to 6.1 μs, where G is the fraction of the excess energy lost during each elastic collision ($2m/M$) and ν_m is assumed to have a mean value of $6.0\times 10^8\ s^{-1}$.[27] Thus, the secondary electron energy degrades in the absence of an electric field, by $e^{-8.2}$ before it is lost. As a result, the average electron energy and implied electric field in the bulk of the plasma can be quite low. In contrast, a positive column has a high bulk electric field (2.5 V/cm for the example in the Appendix) and a high average electron temperature. The high field and temperature are required to produce adequate ionization by electrons in the "tail" of the distribution in the absence of the electron beam. In the rf discharge, the electron beam performs the function of the "tail" of the distribution in a dc discharge, namely, ionization. Thus, while the exact relation between the radiation temperature and the average energy is a function of the electron energy distribution [Eq. (4)], the microwave noise data indicate that the average electron energy is low and that the electron energy distribution is decidedly non-Maxwellian, since a plasma having a Maxwellian distribution with a temperature of only 500 K cannot sustain itself.

Evidence for the existence of electron beam ionization can also be seen in Fig. 9 where the electron density is plotted as a function of the electrode spacing for constant current. While the rf voltage rises with increasing electrode spacing (Fig. 10), the electron density has a peak for electrode spacings of 10–15 cm. The position of the ground electrode was fixed while the position of the driven electrode was varied. The microwave horns were located near the grounded electrode. In the rf discharge, both the ground and the driven electrodes become momentary cathodes during different

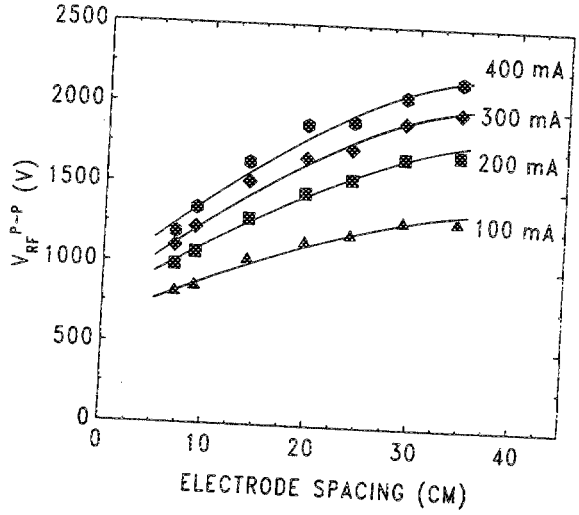

FIG. 10. Peak-to-peak voltage across the rf electrodes as a function of electrode separation for constant peak-to-peak rf current. The electron density is shown in Fig. 9.

phases of the applied voltage. As a result, each electrode will have associated with it an electron beam due to the large sheath potential at the cathode. If the electrode spacing is not too large, a neutral atom in the center of the discharge will have two chances to be ionized during an rf cycle. However, if the electrodes are very close together, a large fraction of the electron beam will strike the anode before it has a chance to lose all of its energy in ionizing or excitative collisions. When the electrode spacing is increased, the beam electrons will propagate further before striking the anode and, as a result, will produce more electrons due to collisional ionization. However, the length over which the beam will propagate is finite. As the spacing is further increased, the beam no longer propagates to the other electrode and does not overlap in the center of the discharge. Since a neutral atom now has only one chance in an rf cycle to be ionized, the electron density will decrease. The electron density will reach an asymptotic value as the bulk field and temperature slowly increase to compensate for the loss of ionization from the electron beam.

The peak of the electron density shifts to larger electrode spacing with increased current. This is due to the increased discharge voltage and the resulting larger cathode sheath voltage increasing the average energy of the electron beam and its mean free path. One would expect the peak electron density when the distance the electron beam propagates is on the same order as the anode to cathode spacing. From the data in Fig. 9, the maximum electron density occurs when the electrode separation is between 10 and 15 cm depending on the rf voltage. If we assume a 200-eV electron to be fairly representative of the electron beam, the total cross section is approximately 4.0×10^{-17} cm^2.[28] The resulting electron mean free path in 0.5 Torr of helium is approximately 1.5 cm. This agrees fairly well with the location of the electron density peak in Fig. 9 since the ballistic electrons will make several (5–10) ionizing and exciting collisions before their energy significantly degrades.

A low average electron temperature implies that the electric field in the bulk of the glow may be small. If the electric field was large (few V/cm), as observed in the pulsed dc positive column, the average electron energy would be much higher. A rough estimate of the magnitude of the bulk electric field can be obtained by assuming that the current is carried by electron drift in the space between the sheaths. In Figs. 9 and 10, when the peak rf voltage is 800 V, the peak current is 200 mA, the power is 28 W, and the electron density is 2.4×10^{11} cm^{-3}. The drift current is

$$I=\int eN_e w_d\, dA\,, \tag{8}$$

where I is the current, e is the electron charge, N_e is the electron density, and w_d is the drift velocity. Since the area of the electrodes is 70 cm^2, the calculated drift velocity using Eq. (8) is 7.4×10^4 cm/s. This corresponds to an E/N of 3.0×10^{-19} V cm^2 or an electric field of 5.3 mV/cm.[29] Thus, the discharge only requires a bulk electric field of a few mV/cm to maintain current continuity, not to maintain itself. In fact, the calculated bulk electric field is so low that the absence of a diffusion-driven current is a serious deficiency of the calculation. Thus, while this calculation is rough, it does serve to illustrate the point that an electron beam sustained plasma can have a low electric field in the bulk of the glow and that this idea is consistent with the observed low radiation temperature.

The calculated low bulk plasma electric field and the plasma voltage drop ($\simeq$53 mV) of the previous example are small when compared with the voltage across the electrodes (800 V). Since only a small fraction of the applied voltage is required to carry the current, the majority of the applied rf voltage is dropped across the cathode sheath. This conclusion is supported by the following calculation based upon the power. If we assume that all of the rf power is deposited in the glow region, not in the sheaths, then we can calculate what the voltage and current should be and compare those numbers with the experimental results. Power is given by

$$P=\int JE\, dV \tag{9a}$$

$$=N(N_e e w_d)E/NV\,, \tag{9b}$$

where N is the neutral density, V is the discharge volume, E is the electric field, and J is the drift current Eq. (8). Since the relationship between the drift velocity and E/N is well known,[29] we can use the data from the previous example to calculate an E/N of approximately 5.0×10^{-17} V cm^2 and a drift velocity of 1.2×10^6 cm/s which is considerably higher than that required for current continuity. Using Eq. (8) and the drift velocity, we calculate a drift current of 3.3 A, approximately 10 times the measured peak value. However, the resulting plasma voltage drop of 10 V is still only 2% of the RMS voltage across the electrodes. Thus, even though the calculated current is too large, the calculated voltage drop is still very small when compared to the voltage across the electrodes.

The positive column view of the helium rf discharge appears to be deficient on several important points. In the previous example, we assume all the power is deposited in the glow and only calculate a plasma voltage drop that is 2% of the applied voltage. However, the calculated current is too high by a factor of 10. Thus, a majority of the voltage and indeed, the power must be expended in the sheath region since the plasma requires only a small amount of the available power and voltage to maintain itself. In addition, the large value of E/N calculated in the positive column example would correspond to a high average electron temperature. While this was observed in the calibration of the microwave system using a pulsed dc discharge, the radiation temperature of the rf discharge was much lower. The calculated electric field between the sheaths required to carry the current by drift is consistent with those for the low radiation temperature and the hypothesis of an electron beam sustained discharge. Finally, measurement of the electron density as a function of electrode spacing, the low radiation temperature, and previous optical diagnostics indicate that the electron beam is a significant source of ionization and the electron energy distribution is decidedly non-Maxwellian. Thus, for the previously described experimental conditions, the helium rf discharge has many important characteristics

that indicate that it should be modeled as an electron beam sustained discharge.

B. Argon, nitrogen, and tetrafluoromethane

Electron density for rf discharges in argon, nitrogen, and CF_4 are shown in Fig. 11. The operating pressure for each gas was chosen to be the lowest pressure at which a discharge could be reliably maintained (0.2 Torr for Ar, 0.09 Torr for N_2, and 0.045 Torr for CF_4). The electron density in argon and nitrogen is less than the electron density in helium for equal currents, while the electron density in CF_4 is very small despite the relatively high input power (Fig. 6). This is partially the result of the electronegative nature of the CF_4 plasma.

The radiation temperature in argon is shown in Fig. 7. Even though the argon pressure (0.2 T) was lower than the helium discharge (0.5 T), the radiation temperature of approximately 800 K was higher than that for helium. The uncertainty in the radiation temperature is due to the uncertainty in the microwave attenuation measurements and thus the emissivity, as was discussed earlier. Since the microwave attenuation in argon was lower (2.6–4.8 dB), the effect of the uncertainty on the radiation temperature is greater.

The slightly higher radiation temperature in argon is possibly the result of several processes. One possible contribution to the higher radiation temperature in argon is due to the longer electron energy relaxation time. As in helium, a secondary electron in argon will have a lifetime, determined by ambipolar diffusion, of approximately 130 μs.[26] However, the electron energy decay time τ_e is 40 μs for an average collision frequency of $8.5\times10^8\ s^{-1}$.[28] Thus, the energy of the secondary electron will only degrade by $e^{-3.2}$ before it is lost. As a result, the average electron energy in argon will be slightly higher than in helium. In addition, the low radiation temperature when compared to a positive column indicates that the electron beam still has a large effect on the characteristics of the plasma.

The electron densities in the N_2 and CF_4 plasmas are lower than the noble gas discharges previously studied. In addition, the radiation temperatures from the nitrogen and CF_4 plasmas were below the detection limit of the microwave noise system due to a combination of low T_r and small emissivity. Using the minimum detectable noise temperature of 300 K, an approximate upper limit on the radiation temperatures for the N_2 and CF_4 plasmas can be calculated. The insertion loss for the N_2 plasma at a current of 500 mA was 1.4 dB, while the CF_4 plasma at a current of 600 mA had an attenuation of only 0.5 dB. The resulting upper limit on the radiation temperature is 1200 K for N_2 and 3000 K for CF_4. However, when the insertion loss is small, a small error in the insertion loss measurement can have a large effect on the calculated temperature. Thus, these values should be treated as rough limits on the actual radiation temperature.

The measured electron density and radiation temperature and the inferred electric field in the bulk of the glow are in contrast with recent theoretical predictions for argon.[13] For example, the predicted electron density is lower than the measured electron density by an order of magnitude while the measured average electron energy (800 K) is lower than the predicted (1.3 eV). In addition, the predicted bulk electric field is a few V/cm as opposed to our inferred value of $\simeq$10 mV/cm. While some of the differences can be explained by a comparison of the theoretical and experimental conditions, there are obvious discrepancies. The measured electron density could be higher due to a larger power loading compared to that obtained in the calculation while the differences in the bulk electric field could be due to the different electron densities (for constant current densities). In addition, the frequency of excitation could have an effect on the characteristics of the plasma by allowing a larger sheath voltage than used in the model. However, the contrast between the measured and calculated average electron energies suggests that these mechanical differences are not the fundamental cause.

While we do not have a complete model at this time, we would like to suggest a physical mechanism which would result in better agreement between the conflicting theoretical calculations and our experimental observations. Some theories conclude that secondary electron emission is not an important mechanism in the rf plasma. However, the models generally preclude the existence of runaway electrons (i.e., a beam) by assuming that the electrons in the sheath are in equilibrium with the local electric field. In contrast, we present experimental evidence for the existence and importance of the electron beam by observing the optical emission (Fig. 8), by measuring a peak in the electron density as a function of electrode spacing (Fig. 9), and a lower than predicted average electron temperature (Fig. 7). The existence of the beam electrons can have a large effect on the characteristics of the rf plasma by providing an additional source of ionization which lowers the required bulk electric field and electron temperature while raising the electron density. While our results may have systematic errors, we believe the possibility has been minimized due to the close agreement be-

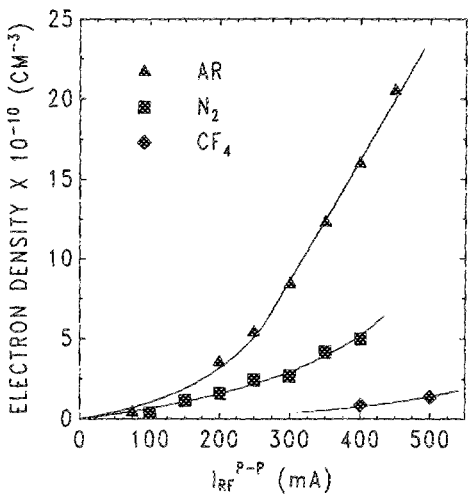

FIG. 11. Electron density as a function of peak-to-peak rf current for argon (0.2 Torr), nitrogen (0.09 Torr), and CF_4 (0.054 Torr). The peak-to-peak rf voltage is 850–1200 V for argon, 1750–2500 V for nitrogen, and 2800–3200 V for CF_4.

tween experimental and theoretical results obtained by calibrating the microwave system against the relatively well-known positive column (see Appendix).

IV. CONCLUSIONS

We have used nonpertubative microwave diagnostic techniques to measure the electron density and electron radiation temperature of radio-frequency plasmas. The existence of the electron beam, apparently produced in the cathode sheath, has a large effect on the characteristics of the rf plasma. The measured radiation temperatures of helium (500 K) and argon (800 K) and the upper limit on the radiation temperatures in N_2 (1200 K) and CF_4 (3000 K) rf plasmas are low when compared to theoretical predictions of several electron volts. Measurements of the electron density as a function of electrode separation show that the electron beam is a significant source of ionization in the discharge. Due to the larger electron density in the rf discharge, the electric field that is required to carry the discharge current by drift is smaller than the typical positive column values, while the measured discharge parameters of rf current, voltage, and radiation temperature do not agree with a calculation based on a positive column theory. Due to the low radiation temperature and electron beam ionization, the electron energy distribution function is non-Maxwellian; thus, the plasma cannot be simply modeled as a time-averaged positive column, but must include more of the features of a negative glow region.

ACKNOWLEDGMENTS

This work was supported by the Joint Services Electronics Program (U. S. Army, U. S. Navy, and U. S. Air Force) and the Army Research Office (Advanced Construction Technology Center).

APPENDIX: MICROWAVE CALIBRATION

Due to the low measured temperature of the rf plasma, great effort was expended in cross checking the accuracy of the microwave radiometry system by using a pulsed dc plasma. A pulsed dc plasma was used since the current requirement for a steady positive column in the system geometry was prohibitively large. The dc plasma was produced by a Velonix hard tube pulser ballasted by a 500-Ω resistor. The discharge voltage was monitored with a Tektronix high-voltage probe. Since it was found that the parallel-plate rf electrodes would not produce a stable discharge, a stainless-steel hollow cathode was used for the pulsed electrode, while the grounded anode was a flat aluminum plate. The use of a hollow cathode and flat anode produced a relatively stable discharge over a wide range of pressures, current, and electrode spacing. The microwave measurements on the pulsed positive column were checked for several pressures and current densities and found to agree with calculated values. The calibration procedure is outlined below for one set of experimental conditions.

The pressure was 1.5 Torr in helium and the high-voltage pulse width was 250 μs at a repetition frequency of 30 Hz. At the end of the 250-μs pulse, the current (2.0 A) and voltage had reached quasisteady-state values. The electric field in the bulk of the glow was measured by monitoring the voltage across the discharge for constant peak current and variable electrode spacing (Fig. 12). The electric field (2.5 V/cm from the slope) divided by pressure is 1.7 V/cm Torr and the cathode voltage drop, extrapolated from the zero crossing, is approximately 250 V. In addition, the electron density and insertion loss reached steady-state values of 1.4×10^{11} cm^{-3} and 3.4 dB, respectively. In order to observe the time-dependent behavior of the plasma temperature, the output of the IF strip was recorded using a boxcar averager which had been calibrated by pulsing the noise tube. The microwave noise from the plasma and the current pulse are shown in Fig. 13. The noise temperature was approximately 30 000 K during the current pulse and fell rapidly at the end of the pulse.

In as much as the pulsed dc discharge is a positive column, the electron density and E/p can be cross checked with the current. An E/p of 1.7 V/cm Torr corresponds to an electron drift velocity of 1.2×10^6 cm/s.[29] The drift current, calculated from Eq. (8), is 1.9 A. This agrees very well with the measured values of 2.0 A. Thus, the measured E/p and electron density (from the microwave phase shift measurement) are consistent with the current.

However, the computed value [Eq. (2)] of the dc plasma attenuation using the measured phase shift (1.2 radians) and a collision frequency ν_m for the positive column of 2.8×10^9 s^{-1} is only 0.56 dB as opposed to the measured insertion loss of 3.4 dB. As discussed earlier, the plasma attenuation measurement is subject to a number of errors from microwave scattering or coupling to many plasma modes.[20] The term plasma mode is used to describe coordinated physical motion of the electrons in the plasma that is driven by the microwave probe. Since the measured scattering is small, a majority of the insertion loss is probably due to plasma modes. While the plasma modes attenuate the microwave probe and make useful collision frequency measurements

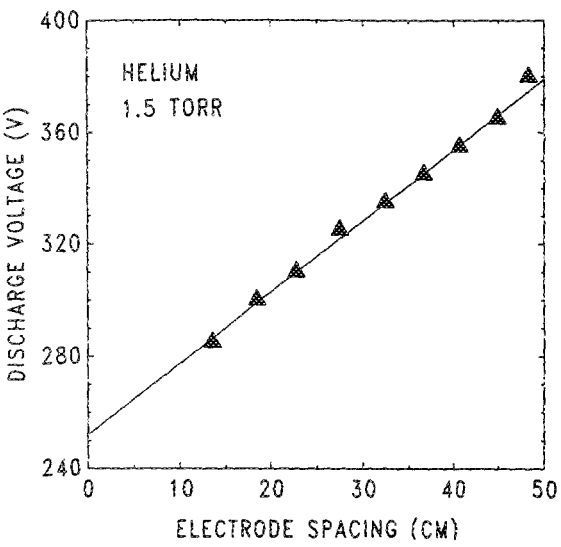

FIG. 12. The discharge voltage across a dc pulsed plasma (1.5-Torr helium) as a function of electrode spacing for a constant peak current of 2.0 A. The cathode voltage drop is 250 V and the electric field is 2.5 V/cm.

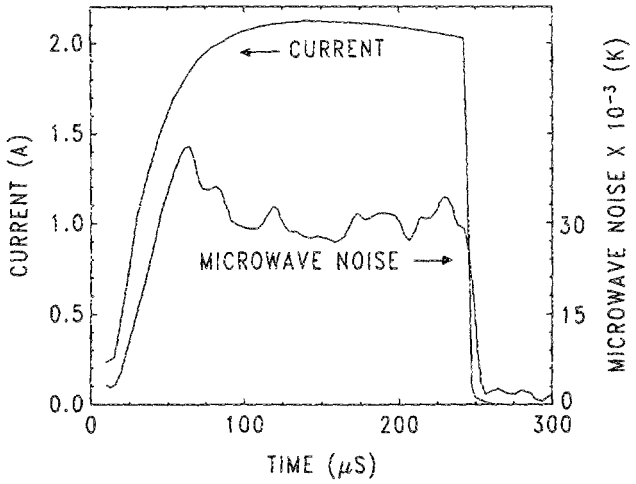

FIG. 13. Discharge current and microwave noise power during the voltage pulse in a 1.5-Torr helium plasma. The microwave noise power, which is independent of electrode spacing, is constant during the current pulse and rapidly decays at the end of the pulse.

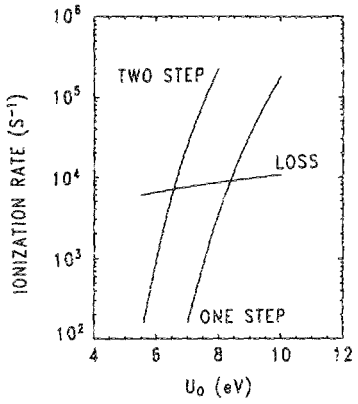

FIG. 14. Calculation of the characteristic energy of a helium positive column (1.5 Torr) using a two-step ionization model of the helium positive column and a Druyvesteyn electron energy distribution. The one-step ionization rate curve includes only ionization from the ground state, while the two-step ionization curve includes ionization from the ground and metastable levels as well as metastable loss due to superelastic collisions. The loss rate is determined by ambipolar diffusion. Due to the Druyvesteyn distribution, the characteristic energy ϵ_k is equal to $u_0/\sqrt{\pi}$.

difficult, they nevertheless radiate microwave noise at their characteristic radiation temperature. Thus, interpreting the measured microwave attenuation as the plasma emissivity [Eq. (3)] leads to a measured value of the radiation temperature (discussed below) that is in agreement with previous measurements[20] and theoretical predictions.

The plasma characteristic energy and radiation temperature were calculated using a two-step ionization model of the positive column and a Druyvesteyn electron energy distribution of the form

$$f_0(u) = Ae^{-(u/u_0)^2}.$$

The Druyvesteyn, as opposed to a Maxwellian, is a closer approximation to the electron energy distribution function of the positive column.[27,30] The model included ionization from the ground and metastable levels as well as metastable production by inelastic collisions and metastable loss through superelastic collisions. All other processes were neglected. The cross sections were assumed to be zero below a threshold energy that depends on the process and have a constant slope above the threshold energy (calculated by using the value of the cross section 1 eV from the threshold energy).[28,31,32] These values were 2.0×10^{-18} cm^2 for ground-state ionization, 2.0×10^{-16} cm^2 for metastable ionization, and 4.0×10^{-18} cm^2 for metastable production. The electron production terms due to ionization were set equal to the losses due to diffusion. The electron loss was assumed to be by ambipolar diffusion, and the metastable loss rate was assumed to be the same as the free ion diffusion loss rate.[26] Since the metastable level diffusion loss rate is small when compared to the rate of ionization from the metastable level and the superelastic loss of metastables, it was neglected.

The results of the calculation for both one- and two-step ionization processes are shown in Fig. 14. At the current densities used in the calibration procedure, two-step ionization is expected to be important.[27,30] The characteristic energy for a Druyvesteyn energy distribution ϵ_k was calculated by dividing the calculated diffusion coefficient D by the calculated mobility μ. As a result, the value of u_0 (Fig. 13) is equal to $\sqrt{\pi}\,D/\mu$ and the calculated characteristic energy is 3.7 eV. The expected value from an E/p of 1.7 V/cm Torr is equal to 2.4 eV.[29] Thus, the calculated characteristic energy agrees with the measured E/p.

The effective radiation temperature of the pulsed dc plasma can be calculated from Eq. (4). Assuming a Druyvesteyn energy distribution and a cross section for momentum transfer that is independent of energy, the calculated radiation temperature is equal to 33 000 K. The calculated value of radiation temperature agrees very well with the measured value if one interprets the measured microwave attenuation (3.4 dB) as the plasma emissivity (Fig. 13). In addition, the calculated and measured radiation temperatures are in good agreement with previous results[20] obtained from both radiometry techniques and probes. Thus, the measured and calculated properties of the pulsed dc positive column are in agreement and the microwave phase shift, insertion loss, and noise power measurement systems are properly calibrated.

[1]D. L. Flamm, V. M. Donnelly, and D. E. Ibbotson, J. Vac. Sci. Technol. B **1**, 23 (1983).
[2]V. M. Donnelly, D. L. Flamm, W. C. Dautremont-Smith, and D. J. Werder, J. Appl. Phys. **55**, 242 (1984).
[3]T. D. Mantei and J. J. Jbara, J. Appl. Phys. **61**, 4885 (1987).
[4]J. Coburn, Plasma Chem. Plasma Process. **2**, 1 (1982).
[5]M. J. Kushner, J. Appl. Phys. **54**, 4958 (1983).
[6]M. J. Kushner, J. Appl. Phys. **58**, 4024 (1985).
[7]F. J. Kampas and M. J. Kushner, IEEE Trans. Plasma Sci. **PS-14**, 173 (1986).
[8]A. Metze, D. W. Ernie, and H. J. Oskam, J. Appl. Phys. **60**, 3081 (1986).
[9]A. M. Pointu, Appl. Phys. Lett. **48**, 762 (1986).
[10]A. M. Pointu, J. Appl. Phys. **60**, 4113 (1986).
[11]A. Garscadden and K. G. Emeleus, Proc. Phys. Soc. **79**, 535 (1962).
[12]B. E. Cherrington, Plasma Chem. Plasma Process. **2**, 113 (1982).

[13]D. B. Graves, J. Appl. Phys. **62**, 88 (1987).
[14]D. B. Graves and K. F. Jensen, IEEE Trans. Plasma Sci. **PS-14**, 78 (1986).
[15]V. A. Godyak, *Soviet Radio Frequency Discharge Research* (Delphic, Falls Church, VA, 1986), pp. 118–140.
[16]G. A. Hebner and J. T. Verdeyen, IEEE Trans. Plasma Sci. **PS-14**, 132 (1986).
[17]V. A. Godyak and A. S. Khanneh, IEEE Trans. Plasma Sci. **PS-14**, 112 (1986).
[18]A. K. Bhattacharya, J. T. Verdeyen, F. T. Adler, and L. Goldstein, J. Appl. Phys. **38**, 527 (1967).
[19]A. Gilardini, *Low Energy Electron Collisions in Gases* (Wiley-Interscience, New York, 1972), pp. 233–297.
[20]G. Bekefi, *Radiation Processes in Plasmas* (Wiley, New York, 1966), pp. 43–99, 133–170.
[21]M. A. Heald and C. B. Wharton, *Plasma Diagnostics with Microwaves* (Wiley, New York, 1965), pp. 117–154, 192–273.
[22]K. Bockasten, J. Opt. Soc. Am. **51**, 943 (1961).
[23]G. A. Hebner and J. T. Verdeyen, Bull. Am. Phys. Soc. **32**, 1148 (1987).
[24]G. Bekefi, J. L. Hirshfield, and S. C. Brown, Phys. Fluids **4**, 173 (1961).
[25]C. B. Opal, W. K. Peterson, and E. C. Beaty, J. Chem. Phys. **55**, 4100 (1971).
[26]E. W. McDaniel and E. A. Mason, *The Mobility and Diffusion of Ions in Gases* (Wiley, New York, 1973), pp. 268–275.
[27]B. Cherrington, *Gaseous Electronics and Gas Lasers* (Pergamon, New York, 1979), pp. 11–19, 144–158.
[28]B. Chapman, *Glow Discharge Processes* (Wiley-Interscience, New York, 1980), pp. 29–48.
[29]J. Dutton, J. Phys. Chem. Ref. Data **4**, 577 (1975).
[30]L. Vriens, J. Appl. Phys. **45**, 1191 (1974).
[31]L. Vriens, Phys. Lett. **8**, 260 (1964).
[32]N. J. Mason and W. R. Newell, J. Phys. B **20**, 1357 (1987).